



Topographic analysis of ceramic vessel surfaces and variability in wall thickness as a means to identify pottery-forming methods

Richard Thér¹

Department of Archaeology, Philosophical Faculty, University of Hradec Králové, Rokitanského 62, 50003 Hradec Králové, Czech Republic

ARTICLE INFO

Keywords:
Pottery forming
Topographic analysis
Surface roughness
Wall thickness
Ceramic technology

ABSTRACT

This paper discusses the use of topographic analysis of ceramic vessel surfaces and variability in wall thickness to identify pottery-forming methods. It builds on a paper in which we addressed this issue by analysing horizontal sections. In this study, we have focused our attention on the area calculation of the relevant phenomena on the 3D representation of the surfaces of vessels. The aim was to improve the approach's applicability to fragmentary archaeological pottery. An experimental dataset of forming methods with different ways of applying rotational motion was used for the analysis. The forming methods included in this dataset can be reliably distinguished based on surface root mean square height (Sq) measured on the outer surface and circular standard deviation (CSD) of the orientation of the relief created by subtracting the outer and inner surfaces of the vessel using at least 900 mm² (30 × 30 mm) of ceramic vessel surface area.

1. Introduction

Forming is one of the basic steps in pottery manufacture, presenting a great variety of combinations of individual techniques. Its use is usually not limited by the ceramic raw materials used, so it provides a valuable source of information, not only on the technology itself but also for addressing the broader issues related to the social networks the potters existed in (e.g., Derenne et al., 2020; Gallay, 2012; Gelbert, 2003; Gomart et al., 2017; Gosselain, 2008, 2002, 2000, 1998; Mayor, 2010; Roux, 2019, 2017, 2011; Roux et al., 2017). Forming is essentially plastic deformation of the clay caused by movement of the hands and other tools (e.g., Rice, 2015; Roux, 2019; Rye, 1981), which gives rise to the characteristic structure of the components of the clay body and specific topography and morphology of the object surface (Thér, 2020). This article is focused on the study of surface topography. The advantage of surface analysis is that the surface is accessible to the naked eye. The analysis can therefore be carried out non-destructively and at relatively low cost. It makes it possible to collect statistically representative data, an essential prerequisite for interpreting technological variability in archaeological pottery analysis. On the other hand, the surface topography is transformed in later stages of forming, which usually obliterates the topography resulting from previous forming stages. For this reason, topography analysis can only provide a particular type of pottery-forming-related information and needs to be incorporated into a more

comprehensive analytical approach.

Besides the analysis of surface residues by visual observation and qualitative description (e.g., Choleva, 2012; Doherty, 2015; Dupont-Delaleuf, 2011; Gomart, 2014, 2011; Jeffra, 2013; Knappett, 1999; Kudelić, 2020; Martineau, 2002; Méry et al., 2012; Rosselló and Trias, 2013; Roux, 2019; Rückl and Jacobs, 2016; Van Doosselaere, 2010) there is also the possibility of quantifying the topographical phenomena. In many cases, quantification reduces the complexity of diagnostic features to only a few aspects that can be measured, meaning that such analysis cannot fully replace qualitative description. On the other hand, it brings an important element of observer independence and repeatability to this analysis area.

In archaeology, the quantitative approach to surface topography has to date been applied mainly to materials other than ceramics (e.g., Evans and Donahue, 2008; Evans and Macdonald, 2011; Faulks et al., 2011; Kimball et al., 1995; Laskaris et al., 2017; Macdonald, 2014; Stemp, 2014; Stemp et al., 2009; Stemp et al., 2015a; Stemp et al., 2015b; Stemp and Stemp, 2001; Zupancich et al., 2025).

We recently published the first attempt to employ quantitative topographical analysis to identify specific aspects of the pottery-forming process. The research question was whether it is possible to distinguish the different contributions of rotational motion in the forming sequence. It was based on the hypothesis that the actual relief of the surface of the ceramic vessel wall is composed of several topographical components

E-mail address: richard.ther@uhk.cz.

¹ ORCID of the author: 0000-0001-6253-5148.

reflecting different aspects of forming the final shape. The most important ones for analysing the forming techniques employed are unintentional deviations from the *ideal form* of the vessel (the potter's idea of the basic vessel shape), reflecting the type of deformation specific to individual forming techniques and mastery of the techniques (Thér, 2020). These unintentional deviations can be treated as geometrical irregularities, which can be measured as deviations from defined reference surfaces (Whitehouse, 2002) – the ideal shape of the vessel.

The topographical analysis in our previous study was based on sections cutting the vessel horizontally. Potters usually intend to achieve a circular shape of a vessel in horizontal sections. Consequently, horizontal sections are optimal for the analysis as the deviations can be measured as the distances between points lying on a horizontal section of the vessel and an ideal circle/ellipse passing through these points (Thér and Wilczek, 2022). Another parameter used to approximate the deviations was the wall thickness. This parameter was calculated as the distance between a given point on one side of the section and the projection along its normal on the other (Thér and Wilczek, 2022).

We hypothesise that the different contributions of rotational movement to the forming sequence as a whole cause different deviations from the ideal form of the vessel. We therefore applied the analysis to the experimental collection of three forming methods utilising rotational movement: *coiling combined with wheel finishing using a turntable (CTF)*, *coiling combined with wheel finishing on a potter's wheel (CWF)* and *wheel throwing (WT)*. The analysis has shown the interesting potential of topographic analysis in distinguishing between different ways of applying rotational movement during pottery forming. However, it was carried out on a whole horizontal section, whereas in archaeology finding whole vessels intact is extremely rare. The analysis's utility has also been demonstrated in smaller portions of the sections (Thér and Wilczek, 2022). However, even if the analysis is applied to an eighth of the vessel circumference, the selection of suitable samples of archaeological pottery will be considerably narrowed. For example, if we consider a vessel with a diameter of 300 mm, an eighth of its circumference is more than 117 mm long.

In addition, the analysis is dependent on determining the axis of symmetry, which is necessary for defining the circle or ellipse representing the ideal shape of the vessel in the horizontal section. The determination of this axis can be uncertain in many cases of fragmentary archaeological pottery. A possible solution to these limitations is to study deviations from the ideal shape not in the sections but in the surface of the samples. Analysing the surface roughness or variability of vessel wall thickness in the area makes it possible to obtain much more data per unit area of the ceramic fragment.

This study explores the potential of topographic surface analysis and wall thickness variability as diagnostic tools for identifying pottery-forming techniques, particularly those involving rotational motion. The primary research objective is to determine whether the forming methods used in our previous study – CTF, CWF, and WT – can be reliably distinguished based on measurable surface characteristics observable on ceramic vessel fragments. Given the fragmentary nature of most archaeological ceramics, the study further investigates whether such distinctions can be made using small surface areas, which would enhance the method's applicability in archaeological contexts. To this end, the research examines the effectiveness of various digital filtering and form removal techniques, including polynomial regression and spline filtering, in isolating topographic signals relevant to forming processes while mitigating the influence of surface treatment, post-depositional alteration, and scanning artifacts. The study assesses whether a combined analysis of surface roughness and wall thickness can offer a robust and non-destructive framework for distinguishing between pottery-forming methods on a quantitative basis.

2. Materials

The analysis was performed on the same experimental series as the

previous study (Thér and Wilczek, 2022), which allows a comparison of the results of both methods. Here I will therefore only summarise the basic facts about the experimental dataset in bullet points:

- One professional potter manufactured 30 experimental bowls.
- Each bowl is approximately 10 cm high, with a maximum diameter of 23 cm.
- Three forming methods were used: CTF, CWF, WT, and 10 bowls were produced using each of them. All the experimental vessels were fabricated from commercial fine-grained clay (Pávek Keramika, product designation: točířská hlíná ROT) and fired in an electric kiln to 800 °C under oxidising conditions.
- Experimental vessels were scanned in 3D using an Artec Space Spider scanning device, with an accuracy of down to 0.05 mm and a 3D resolution of 0.1 mm, and processed in Artec Studio 15 (Artec 3D, 2020). The 3D models were constructed from multiple partial scans, which were acquired from different angles to ensure full surface coverage. These partial scans were first aligned using global registration algorithms, which estimate the relative positions of the scans based on their geometry. Only those parts where alignment and registration values fell within the best class of the registration quality defined by the standards of the scanning device producer (<0.1 "Good results"; Artec 3D 2020) were used for creation of the 3D model. Following registration, the aligned scans were merged into a unified 3D model using the *Sharp Fusion* algorithm within Artec Studio. This method constructs a high-resolution polygonal mesh by integrating overlapping data points from all scans while preserving fine surface details and minimising noise.
- Each 3D model was manually oriented to align its base with the natural surface on which the artefact originally stood.
- From the lower part of each vessel, one surface sample measuring 20 × 20 mm and one measuring 30 × 30 mm were randomly selected. In total, ten samples from each forming method were compared.

The datasets generated and analysed during this study are available in the Mendeley Data Repository: [<https://doi.org/10.17632/b7gxjf9nb.2>]. The repository includes raw surface topography data. All data are licensed under CC-BY 4.0 and are freely available for reuse with appropriate citation.

3. Methods and results

The following part of the article deals with an exploration of the optimal solution for the given task. For that reason, it is unconventionally divided into three chapters according to the successive methods applied, and for the sake of clarity, the results also include a discussion that underpins the next stage of the analysis.

3.1. Surface roughness

3.1.1. Method

This study builds on previous analyses that relied on horizontal sections, where approximating an ideal shape was relatively straightforward. However, the complex and heterogeneous geometry of ceramic vessel forms makes approximating the vessel's ideal shape across its surface and its subsequent removal a more challenging task. For this purpose, the present study employs form removal techniques, widely used in metrology and signal processing, to filter out undesired or distorting patterns in the data and to isolate surface irregularities related to the forming process.

3.1.1.1. Form removal. Form removal is an essential preprocessing step in surface metrology, which distinguishes surface texture components—namely form, waviness, and roughness—based on their wavelength. According to standard definitions (Forbes, 2013; Musolff and

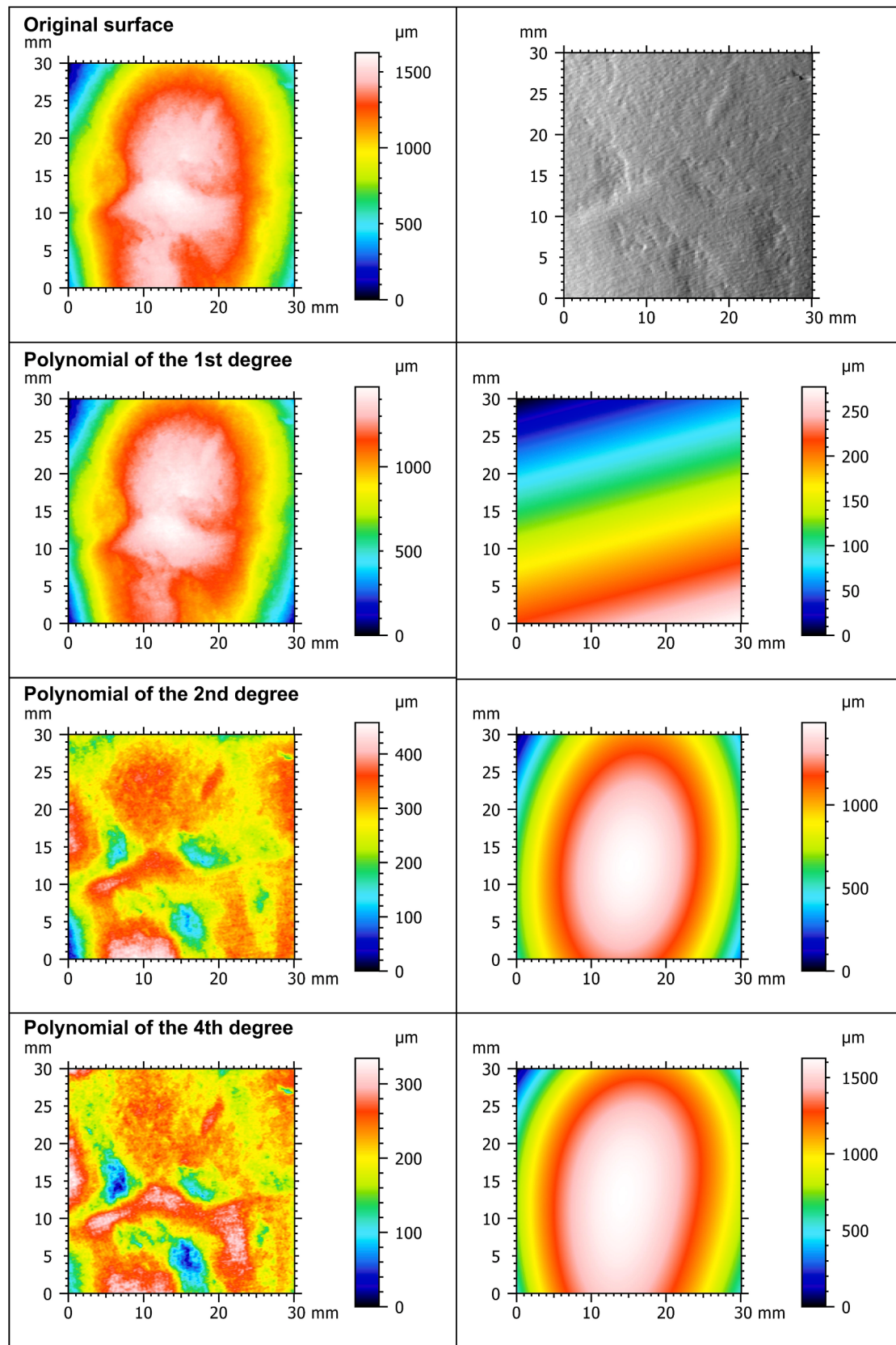


Fig. 1. The effect of shape removal by polynomial regression on the outer surface of an experimental vessel formed by the CTF method. The first pair of images (Original surface) shows an elevation map and a shaded relief of the original 3D representation of the outer surface in a selected 30×30 mm area. The other pair (Polynomial of the nth degree) shows the elevation map of the relief created by removing the shape in the given setting on the left and the elevation map of the removed shape on the right.

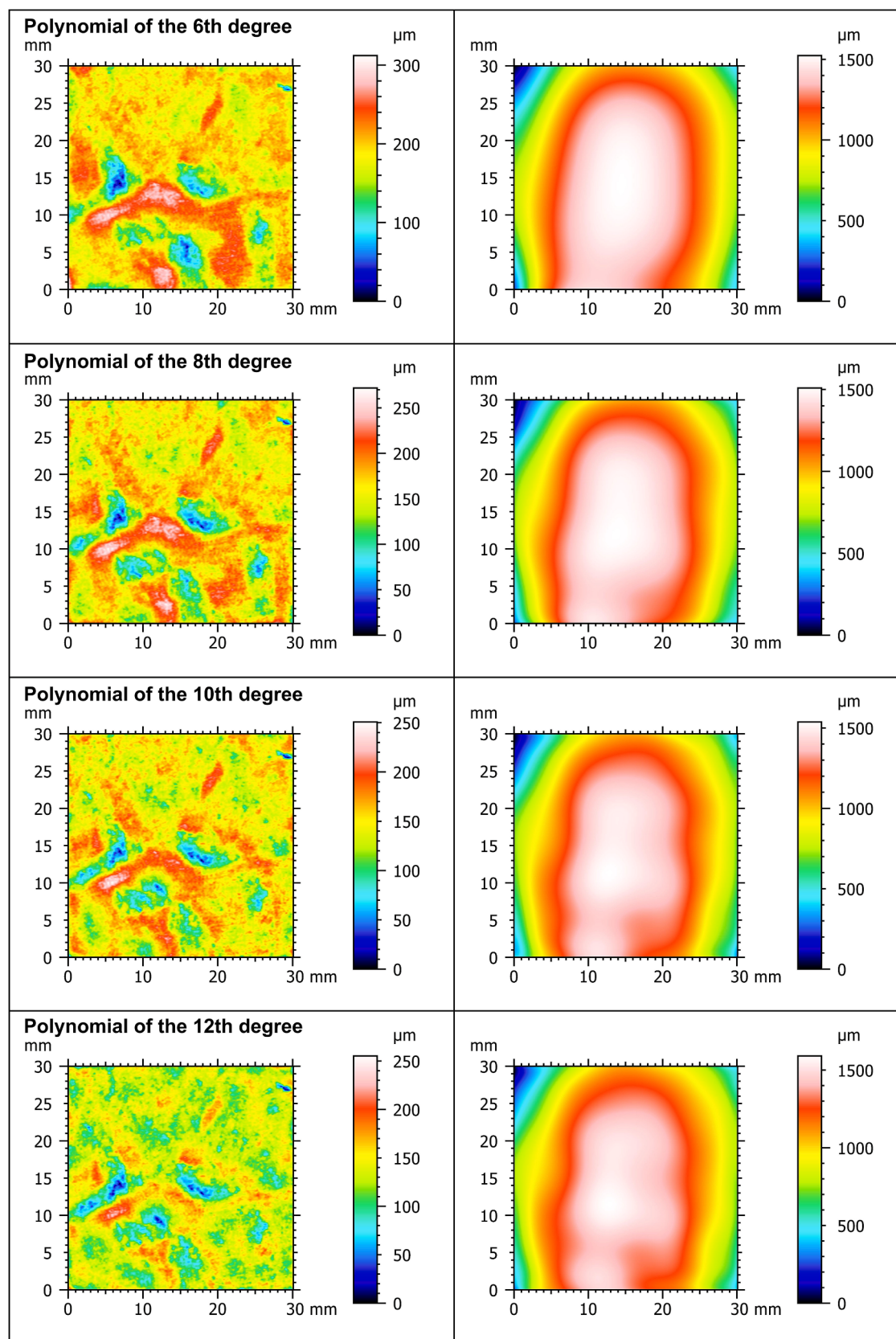


Fig. 1. (continued).

Malburg, 2021), form refers to the long-wavelength geometric component. For irregular objects such as ceramic sherds, polynomial regression is a suitable method for modelling and subtracting this form. In this approach, the measured surface is fitted with an nth-degree polynomial, which is then subtracted to yield the detrended surface. This technique allows for flexible modelling of both linear and complex non-linear trends (e.g., Draper and Smith, 1998; Montgomery et al., 2012; Seber and Lee, 2003). However, selecting the polynomial degree involves balancing the ability to model the overall shape without eliminating relevant surface features. The choice of degree depends on the complexity of the trend which has to be removed. A higher degree allows for modelling more complex structures but increases the risk of so-called *overfitting*, where relevant surface features are removed. After finding the optimal coefficients of the polynomial, the trend modelled by this polynomial is removed from the original data. This is usually done by subtracting the trend values (i.e., the values that the polynomial predicts for each independent variable) from the actual data values. Once the trend has been subtracted from the data, the residuals (differences between the actual and estimated values) are analysed to verify that the trend removed is of an undesirable shape and that the essential characteristics of the data have not been affected.

The optimal degree of the polynomial was determined using a pilot sample of fifteen 30×30 mm areas from experimentally produced ceramics. The polynomial degree was incrementally increased until the residual topography no longer reflected the convex curvature of the vessel surface. This process defined the minimum degree necessary to remove form while preserving pottery-forming-related features. The same setup was applied uniformly to all samples using MountainsMap 7.4 (Digital Surf, 2020). The impact of incrementally increasing the polynomial degree on the shape of the removed form is illustrated using a sample from an experimental vessel produced by coiling with turning (CWT) (Fig. 1).

3.1.1.2. Microtopography removal. To further isolate features resulting from forming procedures, additional filtering was applied to remove microtopography, including surface treatment marks, material-related texture, and post-depositional alterations (Fig. 2A–C). Artefacts from 3D reconstruction, particularly from imperfect alignment of multiple scans, were also considered (Fig. 2D). These residual high-frequency components were addressed using digital filters, which decompose the surface signal into different wavelength bands (Stout and Dong, 1994). The criterion for separation is a wavelength threshold called the *cut-off*. A filter separates large wavelengths above the cut-off into the waviness

part and small wavelengths below the cut-off into the roughness part (Seewig, 2013; Whitehouse, 1994).

This study considered two basic filtering methods for separating waviness from roughness, as well as surface smoothing algorithms as an alternative approach.

1. The Gaussian filter – standardised for profiles (ISO 16610-21, 2011) and areal surfaces (ISO 16610-61, 2015) - works by attenuating high-frequency components of the surface signal, smoothing out short-wavelength features (roughness) while preserving longer-wavelength structures (waviness). At the defined cut-off wavelength, the filter reduces the spectral amplitude by 50 %, and it does so without introducing phase shifts, meaning that it maintains the spatial integrity of surface features. (Muralikrishnan and Raja, 2009a). One major limitation of this filter, however, is its sensitivity to pronounced local deviations, which introduce artificial undulations in the resulting roughness profile. To address this issue, the robust Gaussian filter, defined for profiles (ISO 16610-31, 2016) and areal surfaces (ISO 16610-71, 2014), was developed. It applies robust statistical techniques during filtering to ensure that extreme values do not distort the mean line or bias the results (Markov and Shulepov, 2015; Muralikrishnan and Raja, 2009b). This makes it especially useful for analysing irregular or damaged surfaces.
2. An alternative to the Gaussian filter is the cubic spline filter (for profiles – ISO 16610-22, 2015; for surfaces – ISO 16610-62, 2023). This is a flexible digital filter that works by fitting a smooth spline curve through a series of control points that approximate the surface. Unlike the Gaussian filter, the spline does not pass through the original data points but rather connects suspended points linked to the data by a virtual “spring,” controlled by a tension parameter (β). By adjusting this parameter, the level of smoothing can be finely tuned (Muralikrishnan – Raja 2009c).
3. Another option is to use algorithms to smooth the surface. Smoothing algorithms are computational techniques used to reduce noise and small-scale surface irregularities by averaging or redistributing vertex positions on a 3D mesh or surface. Unlike wavelength-based filters, these algorithms operate directly on the geometry of the surface model, typically by iteratively adjusting each point based on the position of its neighbouring points (e.g., Botsch et al., 2010; Hughes et al., 2019; Schneider and Eberly, 2010). The degree of smoothing is usually controlled by the number of iterations. In this study, the surface smoothing tool in Artec Studio 15 software, as part of the processing workflow for the creation of 3D scans, was used.

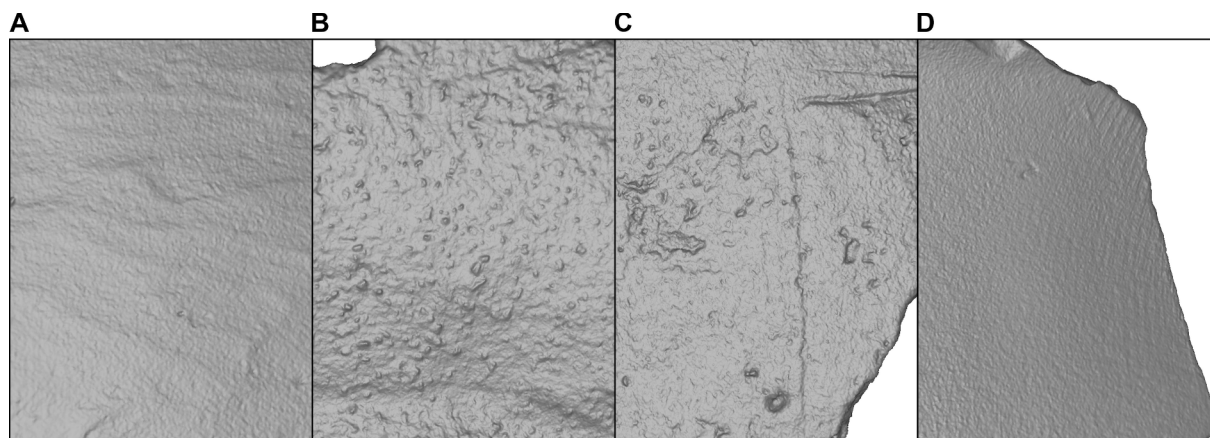


Fig. 2. Examples of topographic phenomena whose influence on the calculation of roughness parameters must be eliminated when studying topography to identify deviations from the ideal shape as evidence of pottery-forming methods. (A) surface treatments, (B) granulometry of ceramic paste, (C) post-production surface damage, (D) artificial texture due to 3D reconstruction error.

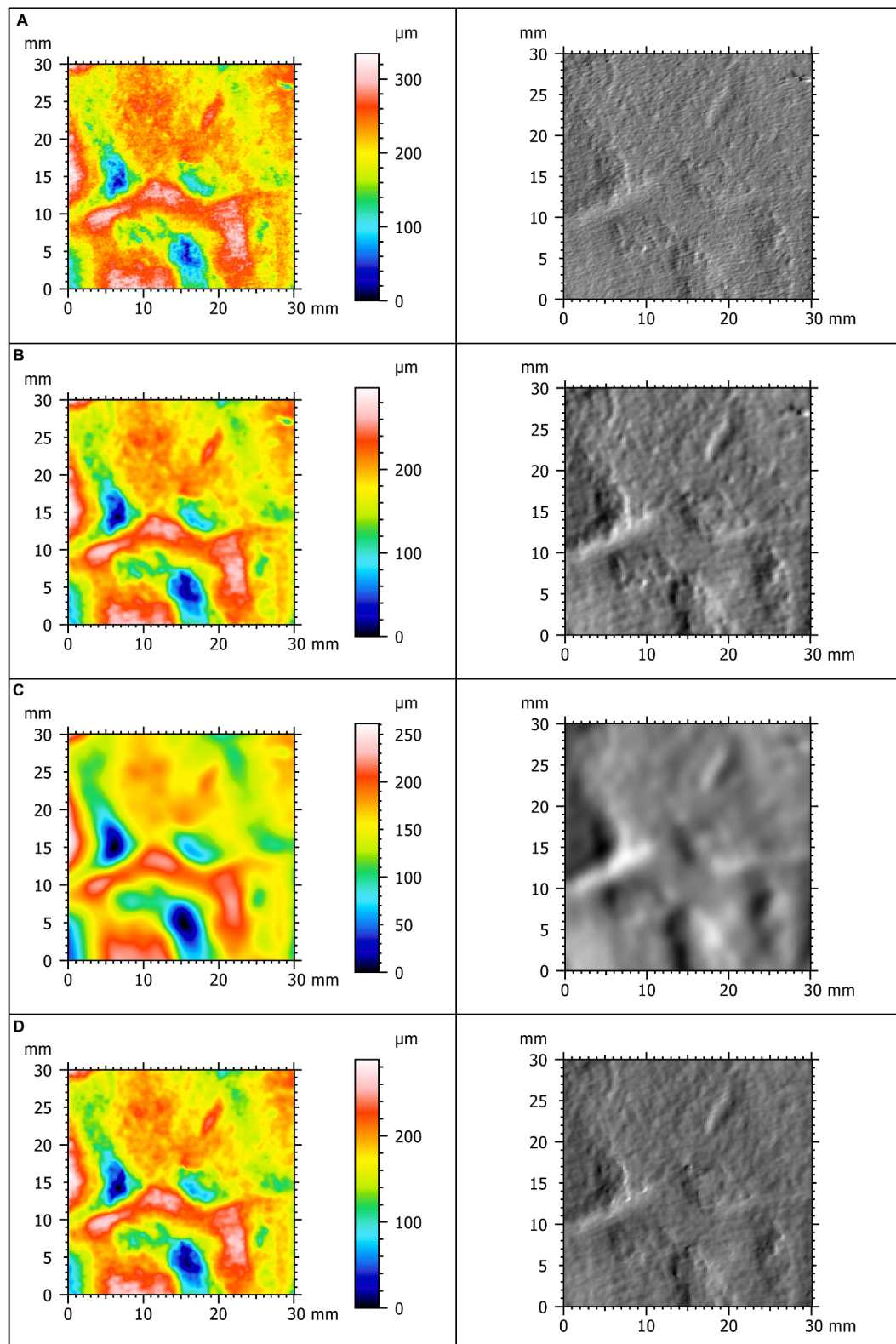


Fig. 3. The effect of smoothing and application of signal filters in removing micro-relief is shown in the example of an experimental sample of the outer surface of a vessel formed by the CTF method. The left side always shows the elevation map, and the right side shows the shading of the relief. (A) 30 x 30 mm area of a 3D scan of the vessel surface taken with the Artec Spider in its original form after reconstruction in Artec Studio 15. (B) Surface smoothing in Artec Studio 15 for 10 iterations. (C) Surface smoothing in Artec Studio 15 for 100 iterations. (D) Roughness removed using a robust Gaussian filter with a cut-off value of 0.8 mm. (E) Roughness removed using a robust Gaussian filter with a cut-off of 2.5 mm. (F) Roughness removed using a robust Gaussian filter with a cut-off of 8 mm. (G) Roughness removed using a spline filter with a cut-off of 2.5 mm. (H) Roughness removed using a spline filter with a cut-off of 8 mm.

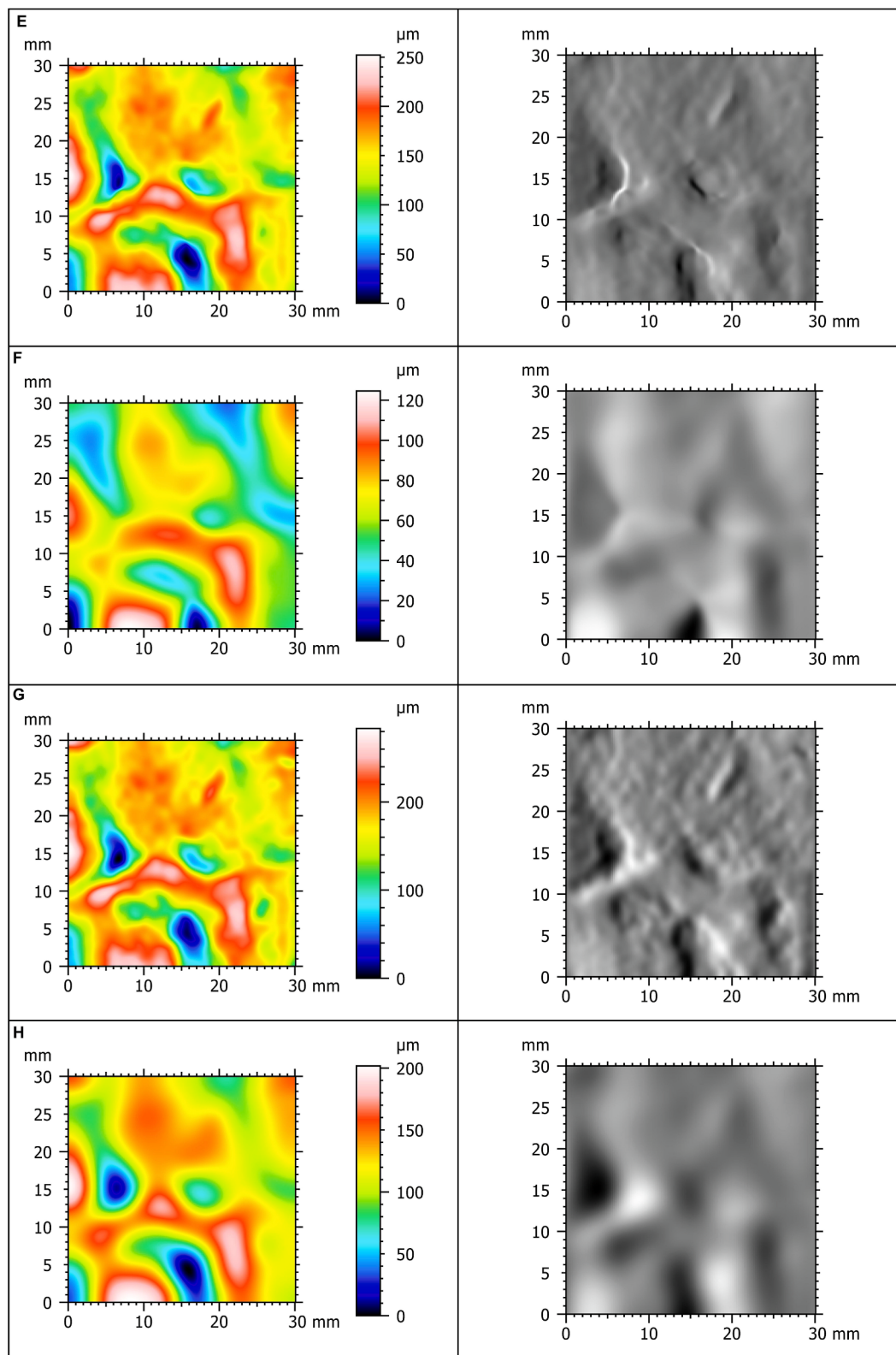


Fig. 3. (continued).

Unfortunately, the specific algorithms underlying this smoothing function are not explicitly described in the available software documentation.

3.1.1.3. Roughness parameters. The effectiveness of these surface-processing approaches in discriminating the three pottery-forming

methods was tested on an experimental collection using the S_q parameter (surface root mean square height), calculated according to ISO 25178-2 ([ISO 25178-2, 2021](#)). S_q is a statistical parameter that expresses the root mean square deviation of the height of the surface points from the mean plane of the measured surface, thus providing information about the variability of the height deviations ([Blateyron, 2013a](#)). The

choice of Sq was based on a combination of theoretical and practical considerations. First, as the second statistical moment of the surface-height probability distribution, Sq is sensitive to the entire range of height deviations by squaring individual differences from the mean, thereby capturing both moderate and extreme variations more effectively than the linear arithmetic mean (Sa). This property aligns well

with the expected nature of forming-related surface irregularities, which are typically dispersed rather than concentrated. Second, Sq enables robust comparative statistical analysis: its additive relationship to variance supports both parametric and non-parametric testing, while avoiding the noise sensitivity and sampling bias inherent in parameters dominated by extreme values (e.g., Sz , Sp , Sv). Third, Sq is inherently

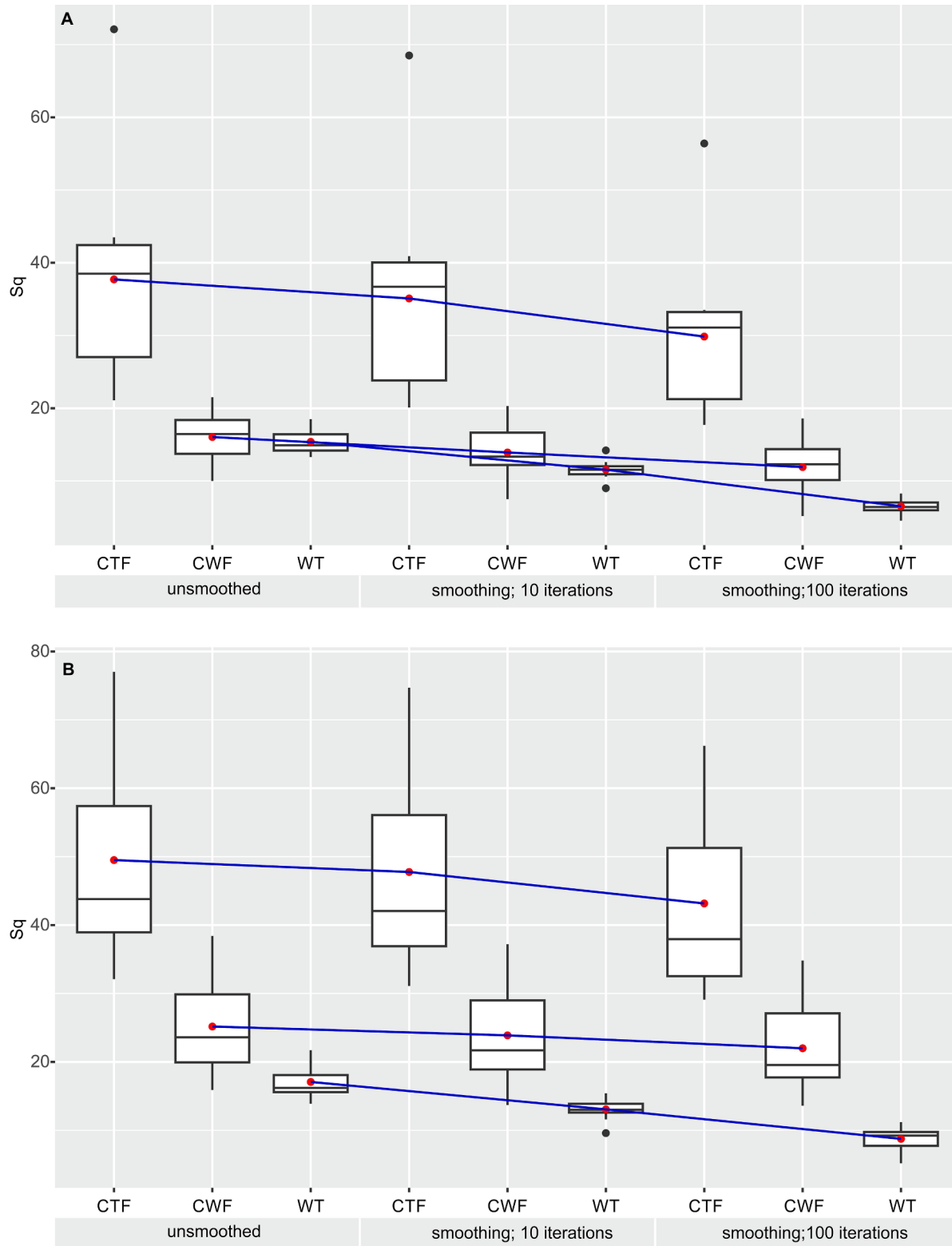


Fig. 4. Comparison of the effect of smoothing on Sq values for 20 × 20 mm (A) and 30 × 30 mm (B) samples. The blue line represents the trend in the change of the arithmetic mean of Sq values, which are marked by red dots.

Table 1

Evaluation of the statistical significance of differences between the different pottery-forming methods for different surface modifications using the Kruskal-Wallis test supplemented by Dunn's paired test with Bonferroni correction.

Untreated, 20x20 mm				Robust Gaussian filter, cut-off 0.8 mm, 30x30 mm			
KW test	df	p-value		KW test	df	p-value	
19.1434	2	0.0001		25.2929	2	0.0000	
group1	group2	Dunn	Corrected p-value	group1	group2	Dunn	Corrected p-value
CTF	CWF	3.5695	0.0005	CTF	CWF	2.5146	0.0179
CTF	WT	3.9760	0.0001	CTF	WT	5.0292	0.0000
CWF	WT	0.4065	1.0000	CWF	WT	2.5146	0.0179
Smoothed, 10 iterations, 20x20 mm				Robust Gaussian filter, cut-off 2.5 mm, 30x30 mm			
KW test	df	p-value		KW test	df	p-value	
20.4942	2	0.0000		25.3063	2	0.0000	
group1	group2	Dunn	Corrected p-value	group1	group2	Dunn	Corrected p-value
CTF	CWF	3.0991	0.0029	CTF	CWF	2.4387	0.0221
CTF	WT	4.4074	0.0000	CTF	WT	5.0298	0.0000
CWF	WT	1.3082	0.2862	CWF	WT	2.5911	0.0144
Smoothed, 100 iterations, 20x20 mm				Robust Gaussian filter, cut-off 8 mm, 30x30 mm			
KW test	df	p-value		KW test	df	p-value	
22.3148	2	0.0000		24.3618	2	0.0000	
group1	group2	Dunn	Corrected p-value	group1	group2	Dunn	Corrected p-value
CTF	CWF	2.7686	0.0084	CTF	CWF	2.2357	0.0381
CTF	WT	4.6990	0.0000	CTF	WT	4.9287	0.0000
CWF	WT	1.9304	0.0803	CWF	WT	2.6930	0.0106
Untreated, 30x30 mm				Spline filter, cut-off 0.8 mm, 30x30 mm			
KW test	df	p-value		KW test	df	p-value	
22.4439	2	0.0000		25.1886	2	0.0000	
group1	group2	Dunn	Corrected p-value	group1	group2	Dunn	Corrected p-value
CTF	CWF	2.6670	0.0115	CTF	CWF	2.6041	0.0138
CTF	WT	4.7244	0.0000	CTF	WT	5.0176	0.0000
CWF	WT	2.0574	0.0595	CWF	WT	2.4135	0.0237
Smoothed, 10 iterations, 30x30 mm				Spline filter, cut-off 2.5 mm, 30x30 mm			
KW test	df	p-value		KW test	df	p-value	
24.0389	2	0.0000		25.8065	2.0000	0.0000	
group1	group2	Dunn	Corrected p-value	group1	group2	Dunn	Corrected p-value
CTF	CWF	2.4895	0.0192	CTF	CWF	2.5400	0.0166
CTF	WT	4.9028	0.0000	CTF	WT	5.0800	0.0000
CWF	WT	2.4133	0.0237	CWF	WT	2.5400	0.0166
Smoothed, 100 iterations, 30x30 mm				Spline filter, cut-off 5 mm, 30x30 mm			
KW test	df	p-value		KW test	df	p-value	
25.0555	2	0.0000		25.5567	2	0.0000	
group1	group2	Dunn	Corrected p-value	group1	group2	Dunn	Corrected p-value
CTF	CWF	2.3876	0.0254	CTF	CWF	2.4895	0.0192
CTF	WT	5.0038	0.0000	CTF	WT	5.0552	0.0000
CWF	WT	2.6162	0.0133	CWF	WT	2.5657	0.0154
alpha = 0.05 Reject Ho if p <= alpha/2				Spline filter, cut-off 8 mm, 30x30 mm			
KW test	df	p-value		KW test	df	p-value	
25.0611	2	0.0000		25.0611	2	0.0000	
group1	group2	Dunn	Corrected p-value	group1	group2	Dunn	Corrected p-value
CTF	CWF	2.3879	0.0254	CTF	CWF	2.3879	0.0254
CTF	WT	5.0044	0.0000	CTF	WT	5.0044	0.0000
CWF	WT	2.6165	0.0133	CWF	WT	2.6165	0.0133

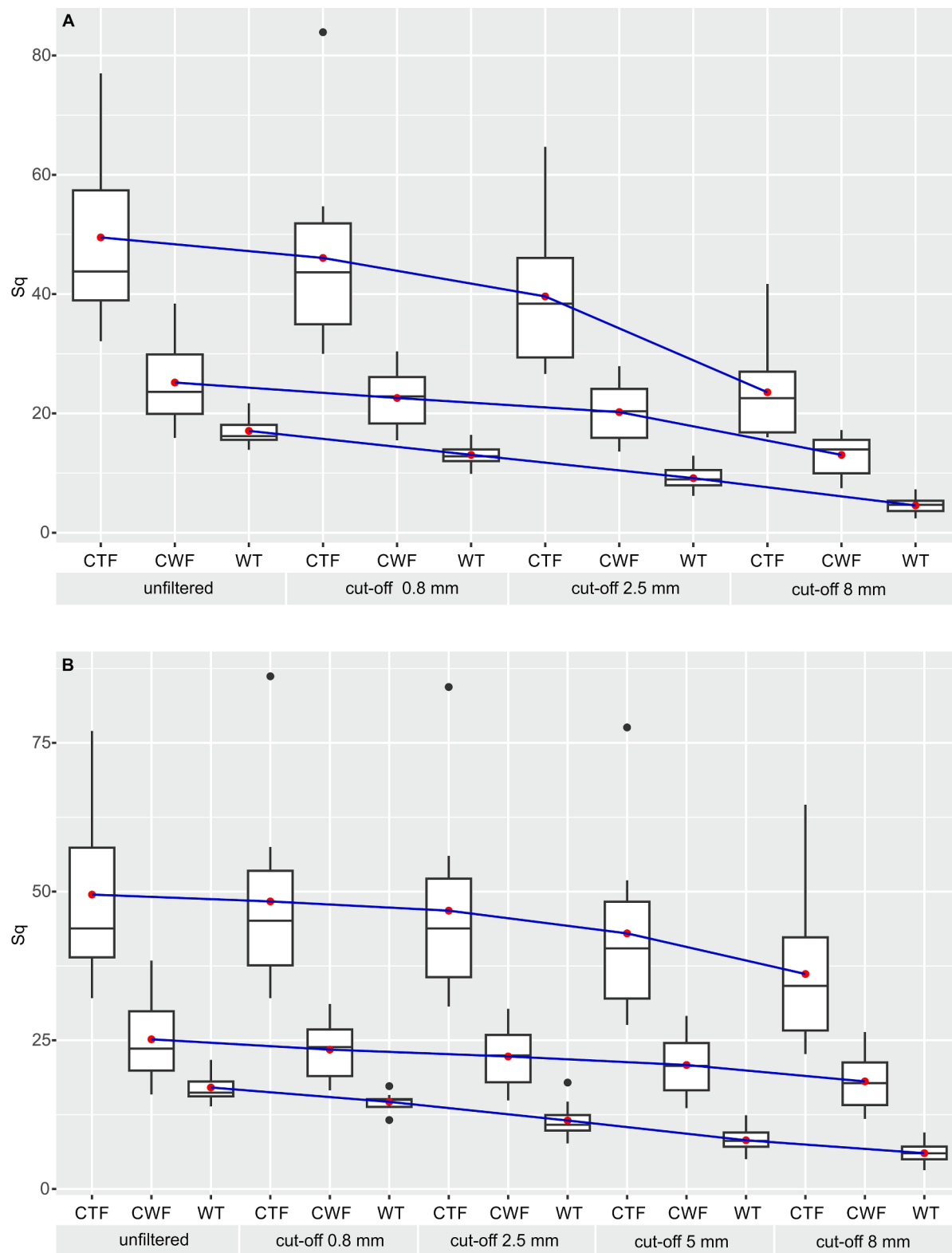


Fig. 5. Comparison of the effect of roughness removal on Sq values using a robust Gaussian filter (A) and a spline filter (B). The analysis is applied to a 30×30 mm area. The blue line represents the trend in the change of the arithmetic mean of Sq values, which are marked by red dots.

orientation-independent, being defined over a detrended areal surface, and is recognised by ISO 25178 as a standardised amplitude metric, facilitating reproducibility and comparability across studies (ISO 25178-2, 2021).

The analysis aims to determine a suitable method for distinguishing

pottery-forming methods in the smallest possible area. This ensures the broadest possible applicability of the technique to fragmentary archaeological ceramics. The initial area size was set at 20×20 mm. The plan was to adaptively increase the analysed area by 10 mm on each side in case of unsatisfactory analysis results.

Table 2

Comparison of the basic statistical parameters exhibited by each pottery-forming method for different surface modifications. *Treatment* – the method of surface transformation used and the area to which the transformation was applied; *Method* – experimentally tested pottery-forming method; *Mean* – arithmetic mean; *CV* – coefficient of variation; *Min.* – minimum value; *QI* – 1st quartile; *QII* – median; *QIII* – 3rd quartile; *Max.* – maximum value. The coloured values in the grey rows relate to the labels in that row, not the column label they are included in. *Mean CTF – mean CWF (% of Avg)* – the difference between the arithmetic means of the *CTF* and *CWF* methods expressed as a percentage of the mean value of the two groups being compared; *Min CTF – max CWF (% of Avg)* – the difference between the minimum value of the *CTF* and the maximum *CWF* expressed as a percentage of the mean value of the two groups being compared, a negative value means that the minimum *CTF* is higher than the maximum *CWF* and there is therefore an overlap in the ranges of variation of the values of the two groups; *Mean CWF – mean WT (% of Avg)* – the difference between the arithmetic mean of *CWF* and *WT* techniques expressed as a percentage of the average value of both compared groups; *Min CWF – max WT (% of Avg)* – the difference between the minimum value of *CWF* technique and the maximum *WT* expressed as a percentage of the average value of both compared groups; a negative value means that the minimum *CWF* value is higher than the maximum *WT* and there is therefore an overlap of the variation ranges of the values of both groups. The best results in the given parameters and the treatment that provides the most reliable overall resolution of the three pottery-forming methods are marked in green.

<i>Treatment</i>	<i>Method</i>	<i>Mean</i>	<i>CV</i>	<i>Min.</i>	<i>QI</i>	<i>QII</i>	<i>QIII</i>	<i>Max.</i>
Untreated, 20x20 mm	CTF	37.71	0.39	21.10	27.03	38.50	42.43	72.10
	mean CTF - mean CWF (% of Avg):	80.63					min CTF - max CWF (% of Avg):	-1.49
	CWF	16.04	0.22	10.00	13.73	16.45	18.38	21.50
	mean CWF - mean WT (% of Avg):	4.20					min CWF - max WT (% of Avg):	-54.11
	WT	15.38	0.11	13.30	14.18	14.90	16.43	18.50
	CTF	35.09	0.41	20.10	23.83	36.70	40.05	68.50
	mean CTF - mean CWF (% of Avg):	86.41					min CTF - max CWF (% of Avg):	-0.82
	CWF	13.92	0.27	7.51	12.20	13.35	16.65	20.30
	mean CWF - mean WT (% of Avg):	18.58					min CWF - max WT (% of Avg):	-52.54
	WT	11.55	0.12	9.00	10.93	11.55	12.03	14.20
Smoothing, 10 iterations, 20x20 mm	CTF	29.85	0.38	17.70	21.25	31.10	33.23	56.40
	mean CTF - mean CWF (% of Avg):	85.93					min CTF - max CWF (% of Avg):	-4.31
	CWF	11.91	0.34	5.19	10.13	12.30	14.38	18.60
	mean CWF - mean WT (% of Avg):	58.48					min CWF - max WT (% of Avg):	-33.43
	WT	6.52	0.16	4.55	5.98	6.43	7.05	8.27
	CTF	49.50	0.30	32.10	38.95	43.80	57.40	77.00
	mean CTF - mean CWF (% of Avg):	65.17					min CTF - max CWF (% of Avg):	-16.87
	CWF	25.17	0.27	15.90	19.93	23.60	29.88	38.40
	mean CWF - mean WT (% of Avg):	38.35					min CWF - max WT (% of Avg):	-27.46
	WT	17.07	0.15	13.90	15.58	16.20	18.08	21.70
Smoothing, 10 iterations, 30x30 mm	CTF	47.76	0.31	31.10	36.90	42.05	56.08	74.70
	mean CTF - mean CWF (% of Avg):	66.67					min CTF - max CWF (% of Avg):	-17.03
	CWF	23.88	0.31	13.70	18.90	21.70	29.00	37.20
	mean CWF - mean WT (% of Avg):	58.59					min CWF - max WT (% of Avg):	-9.20
	WT	13.06	0.13	9.59	12.60	13.00	13.88	15.40
	CTF	43.16	0.32	29.10	32.53	37.95	51.28	66.20
	mean CTF - mean CWF (% of Avg):	64.99					min CTF - max CWF (% of Avg):	-17.50
	CWF	21.99	0.31	13.60	17.73	19.55	27.10	34.80
	mean CWF - mean WT (% of Avg):	86.14					min CWF - max WT (% of Avg):	15.61
	WT	8.75	0.20	5.18	7.72	9.24	9.75	11.20
Robust Gaussian filter, cut-off 0.8 mm, 30x30 mm	CTF	46.06	0.35	30.00	34.95	43.65	51.85	83.90
	mean CTF - mean CWF (% of Avg):	68.38					min CTF - max CWF (% of Avg):	-1.17
	CWF	22.59	0.22	15.50	18.30	22.85	26.10	30.40
	mean CWF - mean WT (% of Avg):	53.49					min CWF - max WT (% of Avg):	-5.05
	WT	13.06	0.14	9.87	12.00	12.80	13.95	16.40
	CTF	39.61	0.30	26.60	29.38	38.40	46.05	64.70
	mean CTF - mean CWF (% of Avg):	64.82					min CTF - max CWF (% of Avg):	-4.35
	CWF	20.22	0.25	13.60	15.90	20.35	24.10	27.90
	mean CWF - mean WT (% of Avg):	75.44					min CWF - max WT (% of Avg):	4.77
	WT	9.14	0.22	6.18	7.95	8.93	10.50	12.90
Robust Gaussian filter, cut-off 8 mm, 30x30 mm	CTF	23.54	0.34	16.00	16.83	22.55	27.00	41.70
	mean CTF - mean CWF (% of Avg):	57.34					min CTF - max CWF (% of Avg):	-6.56
	CWF	13.05	0.27	7.46	9.95	13.95	15.58	17.20
	mean CWF - mean WT (% of Avg):	96.27					min CWF - max WT (% of Avg):	2.04
	WT	4.57	0.34	2.41	3.64	4.67	5.35	7.28

(continued on next page)

Table 2 (continued)

Spline filter, cut-off 0.8 mm, 30x30 mm	CTF	48.35	0.33	32.10	37.60	45.10	53.50	86.20
		mean CTF - mean CWF (% of Avg):	69.40				min CTF - max CWF (% of Avg):	2.79
	CWF	23.44	0.21	16.60	19.00	23.85	26.83	31.10
		mean CWF - mean WT (% of Avg):	44.04				min CWF - max WT (% of Avg):	-6.77
Spline filter, cut-off 2.5 mm, 30x30 mm	WT	14.98	0.12	11.60	14.00	15.00	15.63	17.90
	CTF	46.80	0.34	30.70	35.63	43.80	52.18	84.40
		mean CTF - mean CWF (% of Avg):	70.95				min CTF - max CWF (% of Avg):	1.16
	CWF	22.29	0.23	14.90	17.95	22.45	25.90	30.30
Spline filter, cut-off 5 mm, 30x30 mm		mean CWF - mean WT (% of Avg):	68.78				min CWF - max WT (% of Avg):	1.21
	WT	10.88	0.19	7.67	9.76	10.55	12.30	14.70
	CTF	42.98	0.34	27.60	32.03	40.45	48.30	77.60
		mean CTF - mean CWF (% of Avg):	69.34				min CTF - max CWF (% of Avg):	-4.70
Spline filter, cut-off 8 mm, 30x30 mm	CWF	20.85	0.25	13.60	16.60	20.70	24.55	29.10
		mean CWF - mean WT (% of Avg):	87.10				min CWF - max WT (% of Avg):	8.26
	WT	8.20	0.27	5.03	7.10	8.10	9.51	12.40
	CTF	36.15	0.35	22.70	26.65	34.15	42.33	64.60
Spline filter, cut-off 8 mm, 30x30 mm		mean CTF - mean CWF (% of Avg):	66.59				min CTF - max CWF (% of Avg):	-13.64
	CWF	18.09	0.27	11.80	14.13	17.80	21.28	26.40
		mean CWF - mean WT (% of Avg):	100.04				min CWF - max WT (% of Avg):	19.07
	WT	6.03	0.32	3.16	5.00	6.01	7.15	9.50

The Kruskal–Wallis test, a non-parametric alternative to ANOVA, was employed to assess statistically significant differences in measured parameters among the experimentally replicated pottery-forming methods. Where significant differences were identified, Dunn's post hoc test with Bonferroni correction was applied to perform pairwise comparisons.

3.1.2. Results

Fig. 3 (calculations for individual samples are provided in SM 1) shows the effect of smoothing and two basic types of signal filtering in order to distinguish signals of different wavelengths. The smoothing was applied in ten (Fig. 3B) and 100 iterations (Fig. 3C). The results show that microtopography residuals are still visible even with stronger smoothing, and the resulting surface matches the original topography well. This cannot be claimed in the case of the Gaussian filter. It is more effective in removing microtopography (Fig. 3D–F), but when the cut-off is set to 8 mm, the original surface is deformed and artificial topographic phenomena appear. The spline filter is also effective in removing microtopography. It does not produce artificial edges when applied with a higher cut-off value (Fig. 3G–H). It therefore appears to be the most suitable filter for this purpose.

Using a 20 × 20 mm area, CTF can be reliably distinguished from the other two pottery-forming methods in all topography treatments (Fig. 4A demonstrates it on the smoothed surfaces). A more significant distinction between CWF and WT only occurs when smoothing with 100 iterations is applied. However, in this case, too, the statistical test shows that the difference between CWF and WT is not statistically significant (Table 1 Smoothed, 100 iterations, 20 × 20 mm). In the case of unsmoothed/unfiltered data, the mean values for the two methods are virtually identical. When looking at the analysis of the 30 × 30 mm area, the difference between CWF and WT is already significant when compared to the untreated data (Fig. 4B; Table 1: Untreated, 30 × 30 mm), but it is only at 100 iterations that we observe a sufficiently significant difference between CWF and WT (minimal overlap of maximum and minimum values) to distinguish one from the other. In contrast, the difference between CTF and CWF slightly decreases (Fig. 4B). It is evident that 20 × 20 mm areas cannot be used to distinguish WT from the combined forming methods, while 30 × 30 mm represents a sufficient area for the task.

Regarding the comparison of the methods for removing surface roughness, we observe an increasing difference in the smoothing and spline filter with an increasing number of iterations and increasing cut-off value, respectively (Fig. 4B; Fig. 5B). Both methods achieve similar results. However, better performance is observed in the case of the spline filter (Table 1; Table 2). When using a cut-off value of 8 mm, the differences between CTF and CWF are less pronounced. A cut-off value of 5 mm was therefore included for consideration. This provides the best results in terms of differences between the averages and the maximum and minimum values of the various methods (Table 2). This corresponds to the visual assessment of the results of applying the spline filter: the microtopography is removed, and we do not observe any geometric deformation. As mentioned above, surface deformation occurs at a high cut-off value in the case of the Gaussian filter (Fig. 3F). This is also reflected in the results, with the best values being achieved at a cut-off value of 2.5 mm (Fig. 5A). Even when the transformation results are visually examined (Fig. 3E), it can be seen that, at a given cut-off value, the “cleaning” of the surface is the most effective of all the methods compared, but the Gaussian filter with this cut-off value retains some elements of the microtopography. The spline filter with a cut-off value of 5 mm therefore represents the optimal method for topography analysis to distinguish the applied pottery-forming methods.

3.2. Wall thickness variability

3.2.1. Method

When studying the horizontal profiles, we also considered the wall thickness variability, which – in the case of horizontal sections – proved to be a very effective parameter (Thér and Wilczek, 2022). We therefore also analysed wall thickness variability, which was measured as the distance between the internal and external surfaces of the vessel wall. Before the analysis, the roughness/microtopography of both outer and inner surfaces was filtered using a spline filter with a cut-off value of 5 mm, as this filtering method provided the best results in the evaluation of surface roughness.

The wall thickness can be measured with tools available in industrial metrology software. Either tools are available to measure the thicknesses of whole scanned parts directly, or the difference between two independent surfaces can be calculated. In this study, the *Distance map*

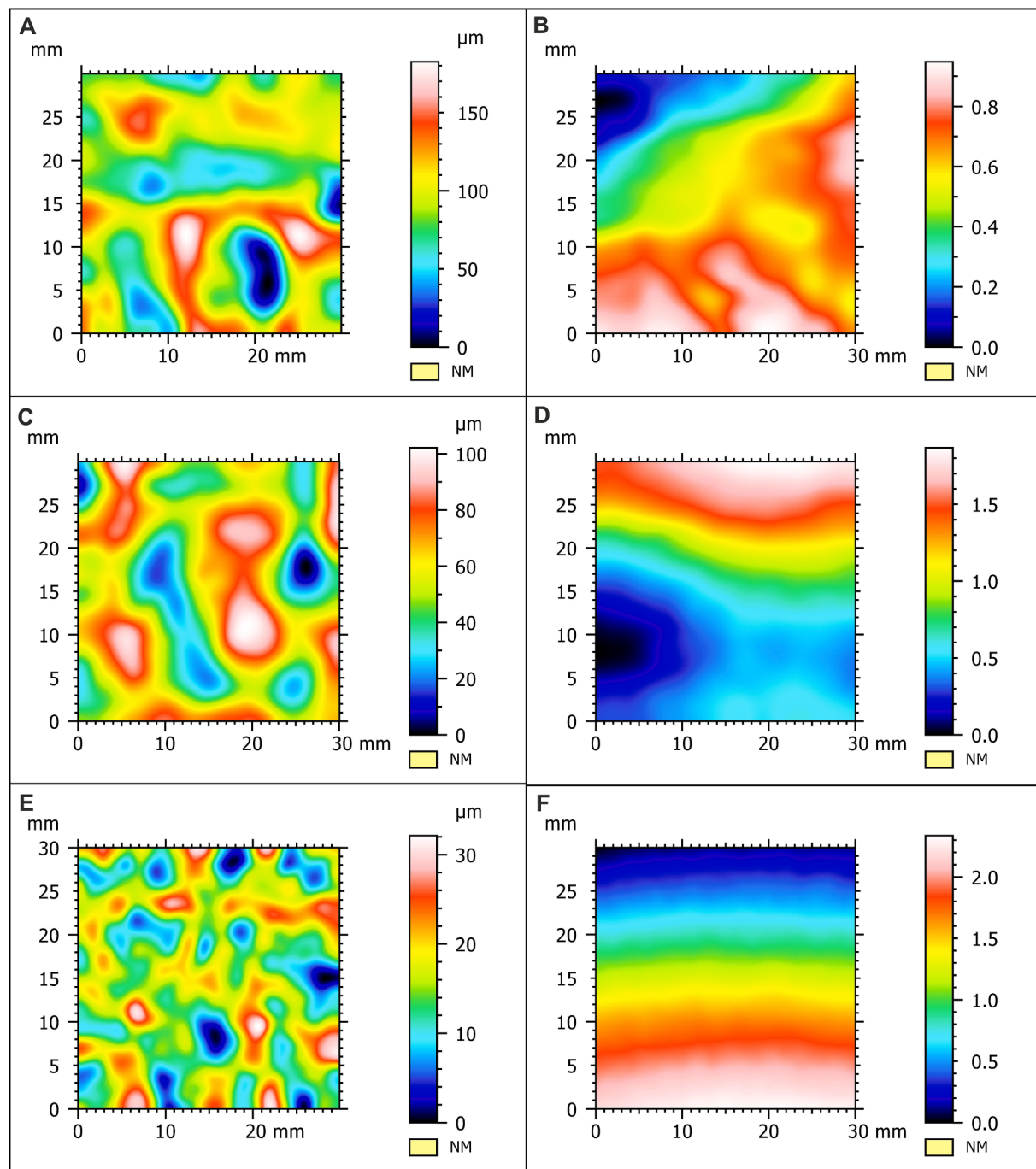


Fig. 6. Comparison of the topography of the surface transformed by the spline filter with a cut-off value of 5 mm (A, C, E) and the difference between the outer and inner surface of the vessel (B, D, F) in the same area for the experimental samples shaped by CTF (A, B), CWF (C, D) and WT (E, F).

tool available in Artec Studio 18 software (Artec 3D, 2024) was used. The tool makes it possible to measure both the thickness (*Thickness*) and the distances between two surfaces (*Distance*). We used the distance tool to perform the analysis on selected areas of the vessel wall (20 × 20 and 30 × 30 mm), as the selection creates two separate surfaces. The tool measures the distance between surfaces along normals or based on the shortest distance between points on the two surfaces. Given the rugged topography of the surfaces, the shortest distance method was chosen as more appropriate for the task. The analysis output is a map of the distances in a given surface, which can be exported as a table of the vertex points of a polygonal 3D surface model with the given distances. The resulting table was imported into MountainsMap 7.4 (Digital Surf, 2020), where the location of the point was defined using the x and y

coordinates determined by the original outer surface, and the calculated distance between the outer and inner surfaces defined its height. This approach produced a relief reflecting the variability in wall thickness (Fig. 6B, D, F). This relief was then analysed in the same way as the topography of the outer surface, except that, in this case, it was no longer necessary to remove the shape. The basic parameter for the evaluation was again *Sq*.

3.2.2. Results

The results demonstrate that, unlike horizontal sections, wall thickness variability alone is not a good indicator (Fig. 7; SM 2). A comparison of the combined methods (CTF and CWF) suggests that the degree of application of rotational motion may affect higher wall uniformity.

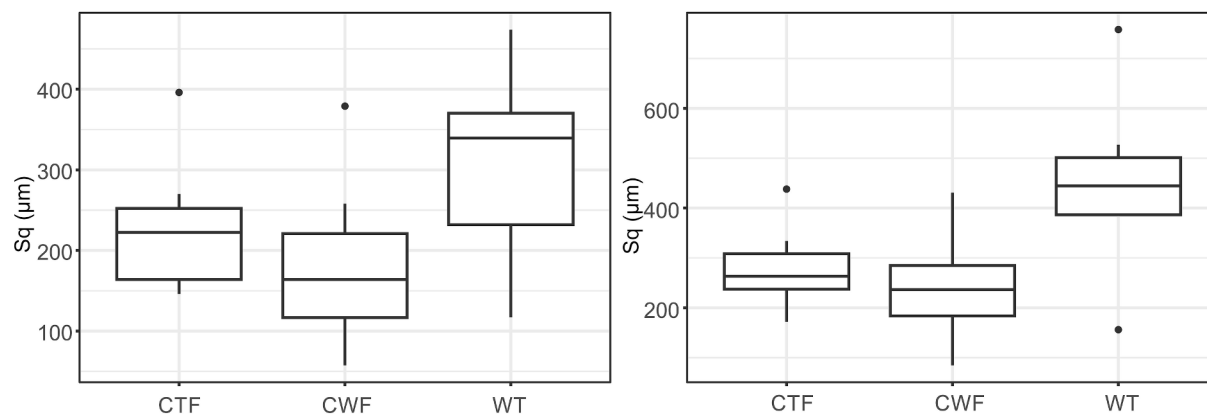


Fig. 7. Comparison of the variability of wall thicknesses of experimental samples in 20 × 20 mm (A) and 30 × 30 mm area (B).

However, the difference in the two datasets is slight, and according to the Kruskal-Wallis test, we cannot claim that there is a statistically significant difference ($H = 2.52$ and $p = 0.1124$ for 20 × 20 mm rafts; $H = 1.65$ and $p = 0.1988$ for 30 × 30 mm rafts). Interestingly, there is significantly higher wall thickness variability in the case of WT. It is exactly the opposite phenomenon to that observed in the case of horizontal sections and also a phenomenon that seems to contradict the initial hypothesis.

However, the initial hypothesis states that uniformity can be expected in a plane parallel to the resultant force vector applied during the deformation of the clay. Its direction is the result of a combination of the upward pull of the fingers and the rotation of the potter's wheel around the vertical axis. Changing finger pressure and the shaping context can affect the wall thickness during throwing. At the moment when the shaped vessel is rotated 360° and the potter's fingers are on the same side of the vessel but in a higher position, the change in pressure can cause a more significant change in thickness in the vector perpendicular to the shaping direction. In other words, the vertical profile of the vessel can be highly variable in terms of thickness. Another source of wall non-uniformity in the direction perpendicular to the forming direction is the shape of the part of the fingers that the potter uses as a working surface during forming. It is rounded and forms a wave-like profile in a direction perpendicular to the forming direction. The result is a typical continuous spiral groove, mostly preserved on the inner surface of the vessel (Courty and Roux, 1995; Rye, 1981). Potters often remove it using a blade in the final stage of shaping. This approach was also used in the case of the experimental collection analysed here. However, despite the use of the blade, the residual topography of the primary forming by finger-pulling may remain visible, especially in the variability of the wall thickness.

We observe a gradual upward thinning of the wall for all WT samples of experimental ceramics. This phenomenon is typical of throwing (Rye, 1981). Potters often deliberately leave thicker vessel bottoms when throwing to enhance the stability of the shaped object, which is in danger of collapsing if the bottom of the vessel cannot support the rapidly growing walls. This phenomenon is also observed in the case of our collection, where it causes a significantly higher variability of surface wall thickness than in combined methods, in which case a more uniform wall thickness in the vertical plane is associated with a successive repetition of coils of the same thickness.

3.3. Directionality of topography

3.3.1. Method

The above-described principle of the formation of non-uniformity in the thickness of the wheel-thrown wall brings the potential importance of another topographic parameter, the directionality of topography. In topographic analysis, directionality can be measured by isotropy analysis. Isotropy in the context of surface texture and surface metrology

means that the surface characteristics are consistent and independent of the direction of measurement. Conversely, anisotropy is a term used to describe materials or systems whose properties vary with direction (Mainsah et al., 2001). In the case of WT, the variability in wall thickness should be strongly anisotropic – the variability will always be low in the direction of the force applied during forming, while it may be high in the direction perpendicular to the direction of the force. In the case of combined forming methods, the different directions of the forming forces are also combined, so these surfaces should be more isotropic. Again, in theory, the degree of anisotropy should correspond to the degree of rotational motion applied during forming.

The basic parameter describing isotropy in metrology is *Str – texture aspect ratio* (ISO 25178-2, 2021). It describes the isotropy or anisotropy of a surface texture and essentially measures the directionality of surface features. The calculation proceeds in the following steps. The direction in which the texture elements (peaks and valleys) are most aligned is determined. This direction is defined as the primary direction. The ratio of the standard deviations of the surface texture profile in two mutually perpendicular directions is calculated: the primary direction and the direction perpendicular to it. *Str* gives an idea of the anisotropy of the surface texture. The parameter is unitless, and its values lie between 0 and 1. It can also be expressed as a percentage between 0 and 100 %. A value close to 1 indicates an isotropic texture where the roughness is similar in all directions. Values significantly less than 1 indicate an anisotropic texture where the roughness varies depending on the measurement direction (Blateyron, 2013a). The problem with applying this analysis to the presented case lies in two points. (a) The measure of isotropy does not consider whether the topographic features' periodicity is in only one direction or in several. For example, surfaces with element periodicity in two directions will also exhibit high anisotropy. (b) The analysis is based on the detection of topographic features (peaks and valleys), but if the difference in thickness varies gradually and uniformly, it is not reflected by these topographic features.

An alternative that addresses both of these problems is to analyse the directionality of changes in wall thickness and calculate the degree of such directionality. In other words, to calculate the directionality of the relief, which is defined by the distance between the outer and inner surfaces (thickness). If the dominant changes in thickness are only in one direction, they will manifest as the uniform directionality of the surfaces defined by these thicknesses. Surface orientation analysis was performed in ArcGIS Pro 3.2 (Environmental Systems Research Institute, 2024). The table of the vertex points of the polygonal 3D surface model with the indicated distances was imported into the ArcGIS Pro environment, where the location of the points was defined using the x and y coordinates of the original position within the 3D model of the outer surface and the height was defined by the distance between the outer and inner surfaces. The raster layer was then interpolated using the Natural Neighbor interpolation method (Natural Neighbor tool) with a

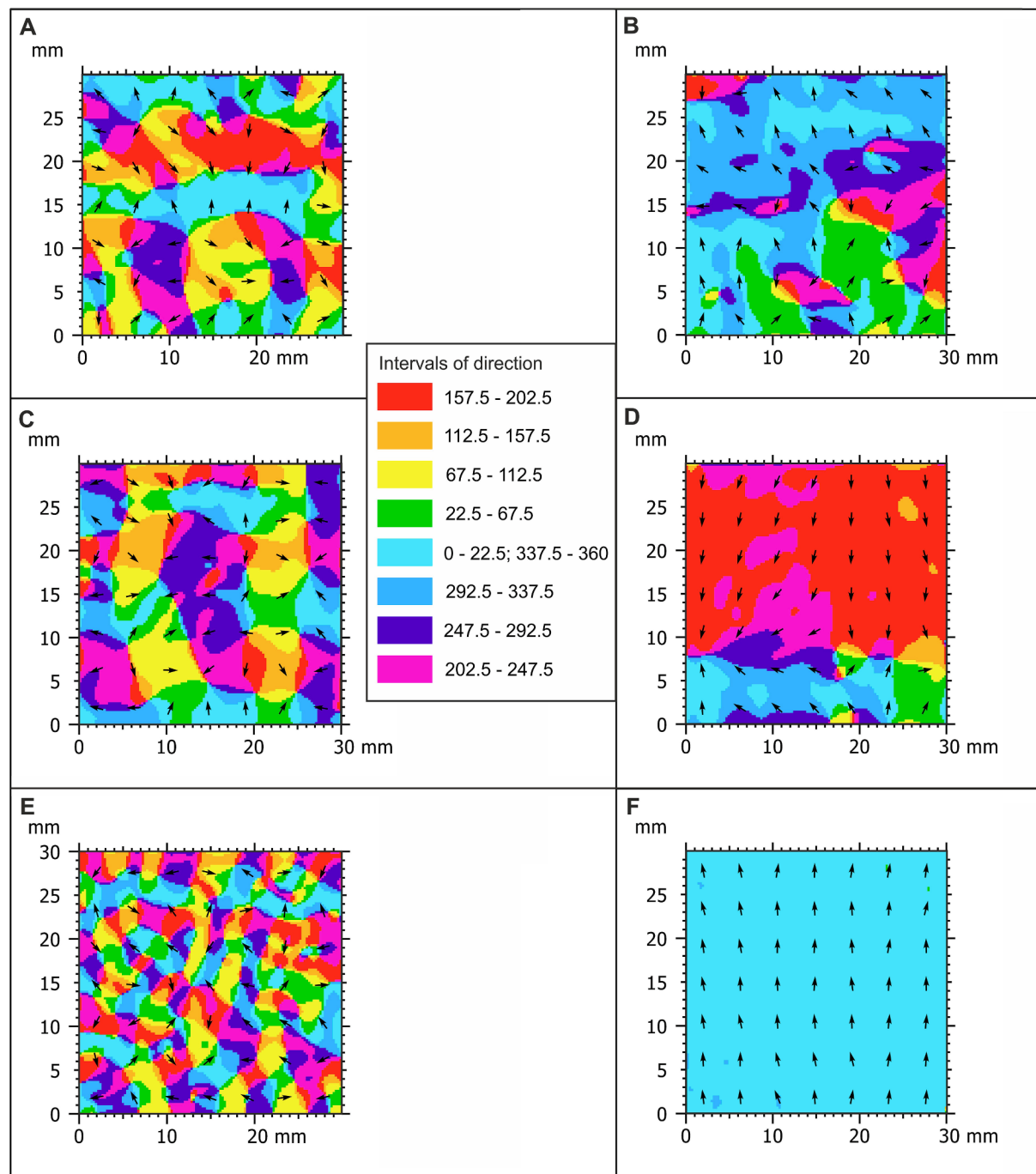


Fig. 8. Comparison of the orientation of the surface transformed by the spline filter with a cut-off value of 5 mm (A, C, E) and the difference between the outer and inner surface of the vessel (B, D, F) in the same area for the experimental samples shaped by CTF (A, B), CWF (C, D) and WT (E, F).

cell resolution of 0.25 mm. The obtained raster was used to calculate the orientation of the surfaces using the *Aspect* tool. It derives orientation for each raster cell based on the surrounding cells' height values. The orientation is expressed in positive degrees from 0 to 360°, measured clockwise from north (Fig. 8). The surface orientation raster was subsequently converted to a point feature class, and its attribute table containing the derived orientation was exported.

As mentioned above, the orientation of the surfaces is expressed in an interval of 0 to 360°. These are what is known as unidirectional circular data, in which case the direction or orientation has an unambiguous interpretation and is only relevant in one direction. If we are to study the

degree of directionality of the topography, however, the orientation expressed in this format is inappropriate. Consider an example from geography. If a mountain ridge is oriented in an east–west direction, then the slopes on the north side of the ridge will face north, and the south slopes will face south. We therefore find two groups of slopes oriented in opposite directions. If we calculate the standard deviation of all the slopes, we get the omnidirectional orientation of all the slopes present. However, the important thing is that all slopes are oriented perpendicular to the ridge axis (i.e. in the north–south axis). If we only account for their axial orientation, we achieve uniform directionality (with a very low standard deviation). The axial data are referred to as

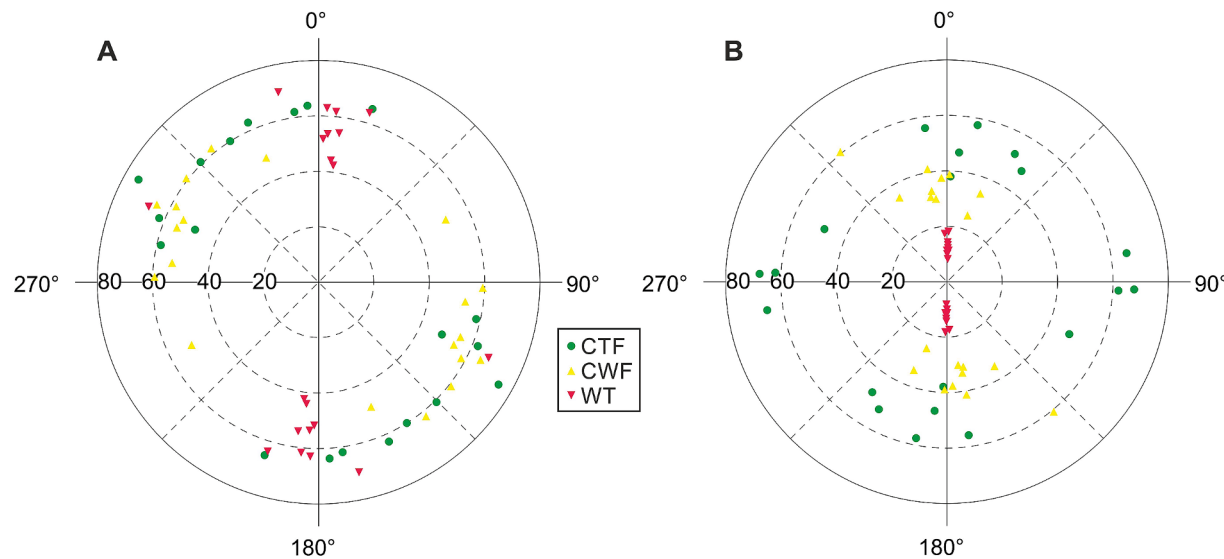


Fig. 9. The polar diagrams show the mean direction of the surfaces and its CSD on samples of the outer surfaces of the experimental vessels with an area of 30×30 mm (A) and the same parameters calculated on the relief based on the distance between the outer and inner surfaces in the same 30×30 mm region (B). The orientation of the surfaces is expressed as an axial (bidirectional) value.

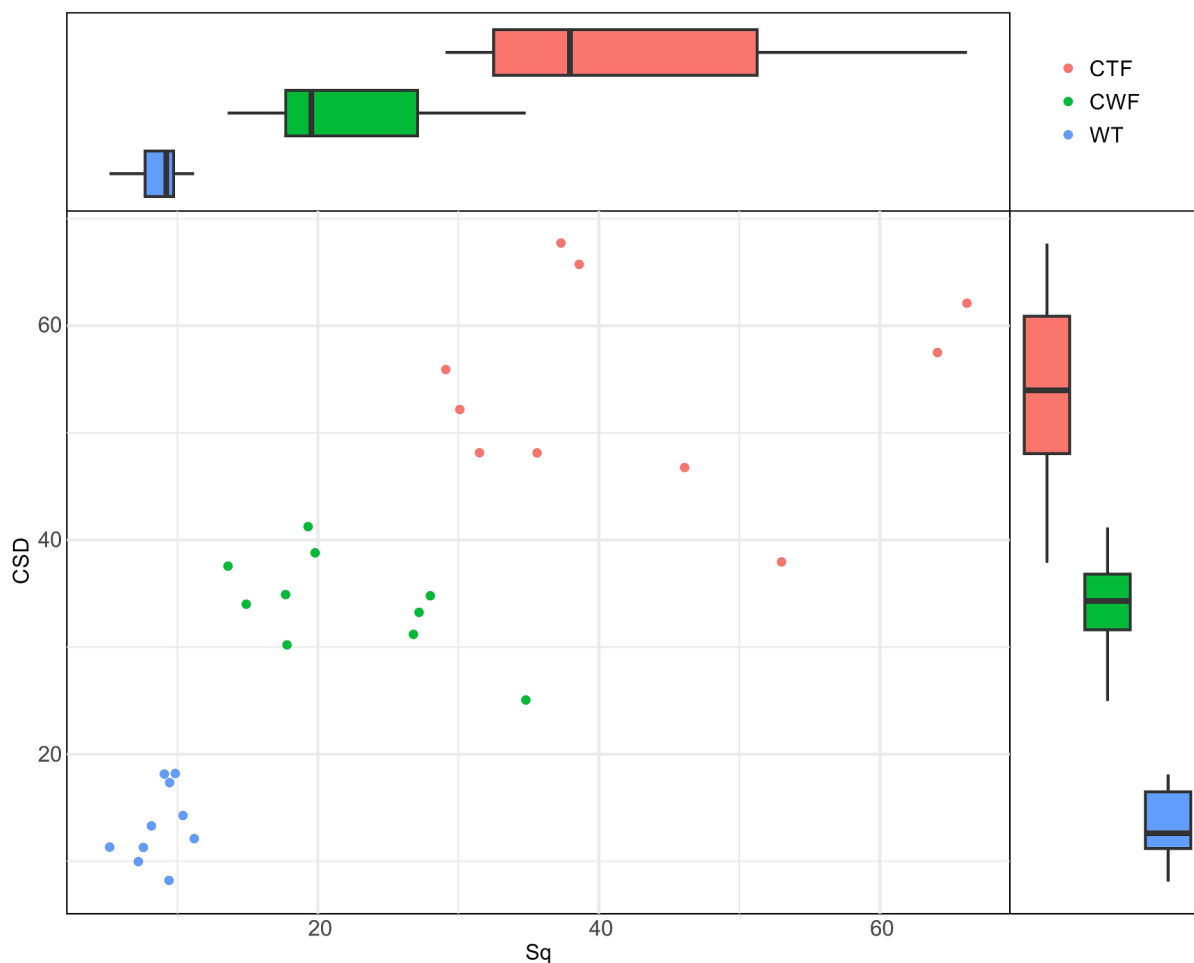


Fig. 10. Scatter plot of Sq and CSD values. Sq is calculated on the outer surface transformed by removing the basic shape of the vessel by subtracting the 4th-degree polynomial, then filtering out the roughness using a spline filter with a cut-off value of 5 mm. CSD is calculated based on axial orientations of the surfaces on the relief representing the distance between the outer and inner surfaces of the vessel. Microroughness is filtered using a spline filter with a cut-off value of 5 mm.

bidirectional circular data and are expressed in an interval of 0 to 180°. Bidirectional circular data help express orientation where orientation is relevant in both directions, and two opposite directions can be considered equivalent (Fisher, 1993; Mardia and Jupp, 2000).

Unidirectional data (slope orientation) can be easily transformed into bidirectional. Angles from 0° to 180° remain unchanged as they are already in the desired range. Angles greater than 181° are transformed by subtracting 180°, i.e. transformed angle = original angle minus 180. Slopes oriented in the opposite direction (e.g. 5° and 185°) thus obtain the same value, which indicates that they are coaxial. All surface orientation results obtained on the experimental samples were converted from unidirectional to bidirectional data in this way.

Two measures of orientation were used for statistical analysis: (a) mean direction – the average orientation of the objects and (b) circular standard deviation (CSD) – the dispersion of values around the mean (Fisher, 1993; Mardia and Jupp, 2000). Statistical analysis of the circular data was performed using Oriana 4.02 (Kovach Computing Services, 2013).

For comparison, the same orientation analysis was performed on the outer surface modified according to the findings described in the *Surface roughness* section.

3.3.2. Results

The comparison of the orientation of the topography of the outer surfaces (Fig. 9A; SM 3) and the orientation of the topography produced by subtracting the outer and inner surfaces (Fig. 9B) shows the importance of evaluating vessel wall thickness for the orientation analysis. Although the topography of the outer surfaces shows a primarily vertical orientation, the alignment is poor, indicating that the surface itself was very well levelled. By contrast, looking at the results of the alignment of the relief representing the difference between the outer and inner surfaces of WT ceramics, we see a high degree of alignment (CSD up to 20°) combined with a strictly vertical orientation that clearly distinguishes WT from the other two methods. The fact that all the shaping in WT is done by the continuous pressure of the fingers in a fixed position (the potter's wheel supplies the energy; the muscular energy is of relatively marginal importance) is reflected in the shape correspondence of the outer and inner surfaces in the direction of the shaping force – and this correspondence is clearly reflected in the directionality of the surfaces. In addition, CTF and CTW can be distinguished based on the degree of alignment.

4. Discussion

The previous sections described the exploration of the optimal topographic analysis solution to differentiate the studied pottery-forming methods on fragmentary archaeological pottery. The results were discussed in the context of the technical logic that gives rise to the specific character of the wall surface topography of ceramic vessels. The necessary surface area for the analysis and the appropriate form and microtopography removal methods were determined so that the roughness analysis expressed through Sq adequately reflects the shape phenomena resulting from the vessel forming. At the same time, the importance of the directionality analysis of the distances between the inner and outer surfaces was shown, representing one of the options for evaluating wall thickness variability. Each of these two useful parameters is more robust in discriminating between different forming methods (although both parameters can discriminate well between all three methods). Simply put, Sq can most reliably distinguish work on potter's wheel and turntable (WT and CWF vs CTF), and directionality can most reliably distinguish wheel-throwing from the combined methods (WT vs CWF and CTF). Consequently, the most robust results can be achieved by combining both of these parameters: combining the two parameters produces clearly distinguishable groups of all analysed methods (Fig. 10).

The results do not represent a universal guide to the analysis of

pottery-forming techniques. The unique combination of the two parameters reflects the theoretical differences in topography due to different ways of applying rotational motion in forming. Even in the case of such a specifically defined group of forming methods, we can expect that the results of the analysis of archaeological pottery will not be so clearly interpretable, as archaeological assemblages will usually comprise a broader range of producers with different skills, styles, tools and materials.

When comparing other forming techniques (e.g. coiling and slab-building), the roughness of the relief expressed by one of the basic parameters, such as Sq , will probably not be a significant factor in distinguishing between them. In these cases, too, it will be necessary to focus on the geometric character of the irregularities. Surface orientation analysis demonstrated here is one of several possibilities. Given the assumptions made, in this study it has only been applied in the schematic form of estimates of the overall surface orientation (expressed by CSD). Other metrological parameters related to roughness analysis (e.g., Blateyron, 2013a) may prove useful in capturing a more specific geometrical character of the relief. Alternatively, topographical analysis can be supplemented by morphological analysis of areal feature parameters (Blateyron, 2013b). The multi-scale fuzzy feature classification used in geography can be particularly helpful in detecting and classifying morphological residues left after shaping (e.g., Fisher et al., 2004; MacMillan et al., 2000; Petry et al., 2005; Schmidt and Hewitt, 2004).

The analysis's most universal outcome is the determination of adequate filtering methods for the different components of the topography, which allows the extraction of relief relevant to the study of the forming practices. These procedures are applicable regardless of the pottery-forming methods and ceramic materials used. Their implementation is limited only by the deep-relief texturing of the surface.

5. Conclusion

It can be concluded that the forming methods applied in the experiment, reflecting different degrees of application of rotational motion in shaping, can be distinguished with a high degree of probability using at least 900 mm² (30 × 30 mm) of ceramic vessel surface area with both surfaces intact. Two measurable parameters have been used. The first is Sq (surface root mean square height), measured on the outer surface and transformed in two steps. First, the basic shape of the vessel was removed employing a 4th-degree polynomial subtraction, then the roughness/microtopography was filtered using a spline filter with a cut-off value of 5 mm. The second significant parameter is the CSD (circular standard deviation) of the orientation of the relief created by subtracting the outer and inner surfaces of the vessel. The orientation was defined as axial/bidirectional circular data, where two opposite directions can be considered equivalent.

It can be assumed that the application to archaeological pottery would yield more ambiguous results than those observed in the experimental dataset, as archaeological assemblages typically reflect a greater diversity of forming techniques, stylistic variation, and individual potters' practices. Nevertheless, this method offers considerable potential as an addition to the portfolio of analytical methods with a non-destructive analysis that provides measurable, repeatable, and reliable parameters that can deepen the scientific argumentation in the complex interpretive task of reconstructing the manufacturing process of pottery forming.

CRediT authorship contribution statement

Richard Thér: Writing – review & editing, Writing – original draft, Visualization, Validation, Methodology, Funding acquisition, Formal analysis, Conceptualization.

Funding

The research leading to these results received funding from the Czech Science Foundation under Grant Agreement No. 23-07619S.

Declaration of competing interest

The authors declare that they have no known competing financial interests or personal relationships that could have appeared to influence the work reported in this paper.

Appendix A. Supplementary data

Supplementary data to this article can be found online at <https://doi.org/10.1016/j.jasrep.2025.105284>.

Data availability

Data will be made available on request.

References

- Artec 3D, 2020. Artec Studio 15 User Guide. Online. Available at: https://docs.artec-group.com/as/15/en/_downloads/25ad86ff3ec13dc8eae3208423c3eb81/Manual-15-EN.pdf [Accessed 27 January 2024].
- Artec 3D, 2024. Artec Studio 18 User Guide. Online. Available at: <https://docs.artec-group.com/as/18/en/> [Accessed 27 January 2024].
- Blateyron, F., 2013a. The Areal Field Parameters, in: Leach, R. (Ed.), Characterisation of Areal Surface Texture. Springer, Berlin, Heidelberg, pp. 15–43. Doi: 10.1007/978-3-642-36458-7_2.
- Blateyron, F., 2013b. The Areal Feature Parameters, in: Leach, R. (Ed.), Characterisation of Areal Surface Texture. Springer, Berlin, Heidelberg, pp. 45–65. Doi: 10.1007/978-3-642-36458-7_3.
- Botsch, M., Kobelt, L., Pauly, M., Alliez, P., Levy, B., 2010. Polygon Mesh Processing. A K Peters, Natick, Mass.
- Courty, M.A., Roux, V., 1995. Identification of wheel throwing on the basis of ceramic surface features and microfabrics. *J. Archaeol. Sci.* 22, 17–50. [https://doi.org/10.1016/S0305-4403\(95\)80161-8](https://doi.org/10.1016/S0305-4403(95)80161-8).
- Derenne, E., Ard, V., Besse, M., 2020. Pottery technology as a revealer of cultural and symbolic shifts: Funerary and ritual practices in the Sion 'Petit-Chasseur' megalithic necropolis (3100–1600 BC, Western Switzerland). *J. Anthropol. Archaeol.* 58, 101170. <https://doi.org/10.1016/j.jaa.2020.101170>.
- Digital Surf, 2020. MountainsMap (Version 7.4.9391) [Computer software]. Digital Surf, Besançon. Available at: <https://www.digitalsurf.com/>.
- Doherty, S.K., 2015. Origins and use of the potter's wheel in ancient Egypt. *Archaeopress Egyptology*, Archaeopress, Oxford.
- Draper, N.R., Smith, H., 1998. Applied regression analysis, 3a, ed. ed. Wiley series in probability and statistics. John Wiley & Sons, New York.
- Dupont-Delaleuf, A., 2011. Styles techniques des céramiques de la protohistoire en Asie Centrale: méthodologie et études de cas. Université Paris Ouest La Défense, Paris. Ph. D. thesis.
- Environmental Systems Research Institute, 2024. ArcGIS Pro (Version 3.2) [Computer software]. ESRI, Redlands, CA. Available at: <https://www.esri.com/>.
- Evans, A.A., Donahue, R.E., 2008. Laser scanning confocal microscopy: a potential technique for the study of lithic microwear. *J. Archaeol. Sci.* 35, 2223–2230. <https://doi.org/10.1016/j.jas.2008.02.006>.
- Evans, A.A., Macdonald, D., 2011. Using metrology in early prehistoric stone tool research: further work and a brief instrument comparison. *Scanning* 33, 294–303. <https://doi.org/10.1002/sca.20272>.
- Faulks, N.R., Kimball, L.R., Hidjrati, N., Coffey, T.S., 2011. Atomic force microscopy of microwear traces on Mousterian tools from Myshtylagy Lagat (Weasel Cave), Russia. *Scanning* 33, 304–315. <https://doi.org/10.1002/sca.20273>.
- Fisher, N.I., 1993. *Statistical analysis of circular data*. Cambridge University Press, Cambridge, New York.
- Fisher, P., Wood, J., Cheng, T., 2004. Where is Helvellyn? Fuzziness of multi-scale landscape morphometry. *Trans. Inst. Br. Geogr.* 29, 106–128. <https://doi.org/10.1111/j.0020-2754.2004.00117.x>.
- Forbes, A.B., 2013. Areal Form Removal, in: Leach, R. (Ed.), Characterisation of Areal Surface Texture. Springer, Berlin, Heidelberg, pp. 107–128. Doi: 10.1007/978-3-642-36458-7_5.
- Gallay, A., 2012. *Potières du Sahel: à la découverte des traditions céramiques de la boucle du Niger (Mali)*. Infolio, Gollion.
- Gelbert, A., 2003. Traditions céramiques et emprunts techniques dans la vallée du fleuve Sénégal. Maison des sciences de l'homme. Epistèmes, Paris.
- Gomart, L., 2011. Pottery traditions and manufacturing organization in the early neolithic: a method for the technological study of Linearbandkeramik vases in habitat contexts in the Aisne Valley (France). *Sprawozdania Archeologiczne* 63, 189–201.
- Gomart, L., 2014. Traditions techniques & production céramique au Néolithique ancien: étude de huit sites rubanés du nord est de la France et de Belgique. Sidestone Press, Leiden.
- Gomart, L., Constantin, C., Burnez-Lanotte, L., 2017. Ceramic production and village communities during the Early Neolithic in north-eastern France and Belgium. issues regarding tempers and pot-forming processes. In: Burnez-Lanotte, L. (Ed.), *Matières à Penser : Sélection et Traitement Des Matières Premières Dans Les Productions Potières Du Néolithique Ancien, Actes De La Table Ronde De Namur (belgique)*, 29 et 30 Mai 2015, Séances De La Société Préhistorique Française. Société préhistorique française, Paris, pp. 133–156.
- Gosselain, O.P., 1998. Social and technical identity in a clay crystal ball. In: Stark, M.T. (Ed.), *The Archaeology of Social Boundaries*. Smithsonian Institution Press, Washington, D.C., London, pp. 78–106.
- Gosselain, O.P., 2000. Materializing identities: an african perspective. *J. Archaeol. Method Theory* 7, 187–217. <https://doi.org/10.1023/A:1026558503986>.
- Gosselain, O.P., 2002. *Poteries du Cameroun méridional: styles techniques et rapports à l'identité*. CNRS éditions, Paris.
- Gosselain, O.P., 2008. Mother Bella was not a Bella: inherited and transformed traditions in Southwestern Niger. In: Stark, M.T., Bowsler, B.J., Horne, L. (Eds.), *Cultural Transmission and Material Culture: Breaking down Boundaries*. University of Arizona Press, Tucson, pp. 150–177.
- Hughes, J.F., Van Dam, A., McGuire, M., Sklar, D.F., Foley, J.D., Feiner, S.K., Akeley, K., 2019. Computer graphics principles and practice, Third, edition. ed. Pearson, Noida, Uttar Pradesh.
- Choleva, M., 2012. The first wheelmade pottery at Lerna: wheel-thrown or wheel-fashioned? *Hesperia the Journal of the American School of Classical Studies at Athens* 81, 343–381. <https://doi.org/10.2972/hesperia.81.3.0343>.
- ISO 16610-21, 2011. Geometrical product specifications (GPS) – Filtration – Part 21: Linear profile filters: Gaussian filters. International Organization for Standardization.
- ISO 16610-22, 2015. Geometrical product specifications (GPS) – Filtration – Part 61: Linear areal filters: Gaussian filters. International Organization for Standardization.
- ISO 16610-31, 2016. Geometrical product specifications (GPS) – Filtration – Part 31: Robust profile filters: Gaussian regression filters. International Organization for Standardization.
- ISO 16610-61, 2015. Geometrical product specifications (GPS) – Filtration – Part 61: Linear areal filters: Gaussian filters. International Organization for Standardization.
- ISO 16610-62, 2023. Geometrical product specifications (GPS) – Filtration – Part 62: Linear areal filters: spline filters. International Organization for Standardization.
- ISO 16610-71, 2014. Geometrical product specifications (GPS) – Filtration – Part 71: Robust areal filters: Gaussian regression filters. International Organization for Standardization.
- ISO 25178-2, 2021. Geometrical product specifications (GPS) – Surface texture: Areal – Part 2: Terms, definitions and surface texture parameters. International Organization for Standardization.
- Jeffra, C.D., 2013. A re-examination of early wheel potting in Crete. *Annual of the British School at Athens* 108, 31–49. <https://doi.org/10.1017/S0068245413000038>.
- Kimball, L.R., Kimball, J.F., Allen, P.E., 1995. Microwear polishes as viewed through the atomic force microscope. *Lithic Technol.* 20, 6–28.
- Knappett, C., 1999. Tradition and innovation in pottery forming technology: wheel-throwing at Middle Minoan Knossos1. *Annual of the British School at Athens* 94, 101–129. <https://doi.org/10.1017/S006824540000538>.
- Kovach Computing Services, 2013. Oriana (Version 7.4) [Computer software]. Kovach Computing Services, Anglesey, Wales. Available at: <https://www.kovcomp.co.uk/oriana/>.
- Kudelić, A., 2020. Trace evidence of pottery forming techniques: early Urnfield culture vessels. In: Miloglav, I. (Ed.), *Recent Developments in Archaeometry and Archaeological Methodology in South- Eastern Europe*. Cambridge Scholars Publishing, Newcastle upon Tyne, pp. 58–81.
- Laskaris, N., Liritzis, I., Bonini, M., Ridi, F., Kersting, R., Al-Otaibi, F., 2017. AFM and SIMS surface and cation profile investigation of archaeological obsidians: New data. *J. Cult. Herit.* 25, 101–112. <https://doi.org/10.1016/j.culher.2016.11.014>.
- Macdonald, D.A., 2014. The application of focus variation microscopy for lithic use-wear quantification. *J. Archaeol. Sci., Lithic Microwear Method: Standard*. Calibr. Innov. 48, 26–33. <https://doi.org/10.1016/j.jas.2013.10.003>.
- MacMillan, R.A., Pettapiece, W.W., Nolan, S.C., Goddard, T.W., 2000. A generic procedure for automatically segmenting landforms into landform elements using DEMs, heuristic rules and fuzzy logic. *Fuzzy Set. Syst.* 113, 81–109. [https://doi.org/10.1016/S0165-0114\(99\)00014-7](https://doi.org/10.1016/S0165-0114(99)00014-7).
- Mainsah, E., Greenwood, J.A., Chetwynd, D.G., 2001. *Metrology and properties of engineering surfaces*. Kluwer Academic Publishers, Boston.
- Mardia, K.V., Jupp, P.E., 2000. Directional statistics. J. Wiley, Chichester; New York.
- Markov, B.N., Shulepov, A.V., 2015. Robust filtering algorithms for roughness profiles. *Meas. Tech.* 58, 730–735. <https://doi.org/10.1007/s11018-015-0784-1>.
- Martineau, R., 2002. Poterie, techniques et sociétés. *Etudes analytiques et expérimentales à Chalain et Clairavaux (Jura), entre 3200 et 2900 av.J.-C.* Bulletin De La Société Préhistorique Française 99, 150–153.
- Mayor, A., 2010. Ceramic traditions and ethnicity in the Niger Bend, West Africa. *Ethnoarchaeology* 2, 5–48. <https://doi.org/10.1179/eth.2010.2.1.5>.
- Méry, S., Dupont-Delaleuf, A., van der Leeuw, S.E., 2012. Les techniques de façonnage céramique mettant en jeu la rotation à Hili (Émirats arabes unis) à la fin du IIIe millénaire (âge du Bronze ancien). *Nouvelles De L'archéologie* 119, 52–64.
- Montgomery, D.C., Peck, E.A., Vining, G.G., 2012. Introduction to linear regression analysis, Fifth edition. ed, Wiley series in probability and statistics. Wiley : A John Wiley & Sons, Inc., Hoboken, NJ.

- Muralikrishnan, B., Raja, J. (Eds.), 2009a. Gaussian Filter, in: Computational Surface and Roundness Metrology. Springer, London, pp. 33–38. doi: 10.1007/978-1-84800-297-5_5.
- Muralikrishnan, B., Raja, J. (Eds.), 2009b. Robust Filters, in: Computational Surface and Roundness Metrology. Springer, London, pp. 87–92. doi: 10.1007/978-1-84800-297-5_11.
- Musolff, C., Malburg, M.C., 2021. The Surface Texture Answer Book. Digital Metrology Solutions, Incorporated.
- Petry, F.E., Robinson, V.B., Cobb, M.A. (Eds.), 2005. Fuzzy Modeling with Spatial Information for Geographic Problems. Springer, Berlin, Heidelberg. doi: 10.1007/b138243.
- Rice, P.M., 2015. Pottery analysis: a sourcebook, second edition. University of Chicago Press, Chicago, London.
- Rosselló, J.G., Trias, M.C., 2013. Making pots: el modelo de la cerámica a mano y su potencial interpretativo. Archaeopress, Oxford, BAR international series.
- Roux, V., 2011. Anthropological interpretation of ceramic assemblages: foundations and implementations of technological analysis. In: Scarcella, S. (Ed.), Archaeological Ceramics: A Review of Current Research. Archaeopress, Oxford, pp. 80–88.
- Roux, V., 2017. Ceramic manufacture: the chaîne opératoire approach. In: Hunt, A.M.W. (Ed.), The Oxford Handbook of Archaeological Ceramic Analysis. Oxford University Press, Oxford, pp. 101–114.
- Roux, V., 2019. Ceramics and society: a technological approach to archaeological assemblages. Springer, Cham. <https://doi.org/10.1007/978-3-030-03973-8>.
- Roux, V., Bril, B., Cauliez, J., Goujon, A.-L., Lara, C., Manen, C., de Saulieu, G., Zangato, E., 2017. Persisting technological boundaries: Social interactions, cognitive correlations and polarization. *J. Anthropol. Archaeol.* 48, 320–335. <https://doi.org/10.1016/j.jaa.2017.09.004>.
- Rückl, Š., Jacobs, L., 2016. “With a little help from my wheel”: wheel-coiled pottery in Protogeometric Greece. *Hesperia: J. Am. School Class. Stud. Athens* 85, 297–321. <https://doi.org/10.2972/hesperia.85.2.0297>.
- Rye, O.S., 1981. Pottery technology: principles and reconstruction. Taraxacum, Washington, D.C.
- Seber, G.A.F., Lee, A.J., 2003. Linear regression analysis, second edition. Wiley series in probability and statistics, Wiley-Interscience, Hoboken, N.J.
- Seewig, J., 2013. Areal Filtering Methods. In: Leach, R. (Ed.), Characterisation of Areal Surface Texture. Springer, Berlin, Heidelberg, pp. 67–106. https://doi.org/10.1007/978-3-642-36458-7_4.
- Schmidt, J., Hewitt, A., 2004. Fuzzy land element classification from DTMs based on geometry and terrain position. *Geoderma* 121, 243–256. <https://doi.org/10.1016/j.geoderma.2003.10.008>.
- Schneider, P.J., Eberly, D.H., 2010. Geometric tools for computer graphics, Transferred to Digital printing, ed. Morgan Kaufmann Series in Computer Graphics and Geometric Modeling. Morgan Kaufmann Publishers, Amsterdam [etc].
- Stemp, W.J., Watson, A.S., Evans, A.A., 2015a. Surface analysis of stone and bone tools. *Surf. Topogr. Metrol. Prop.* 4, 013001. <https://doi.org/10.1088/2051-672X/4/1/013001>.
- Stemp, W.J., Morozov, M., Key, A.J.M., 2015b. Quantifying lithic microwear with load variation on experimental basalt flakes using LSCM and area-scale fractal complexity (Asfc). *Surf. Topogr. Metrol. Prop.* 3, 034006. <https://doi.org/10.1088/2051-672X/3/3/034006>.
- Stemp, W.J., 2014. A review of quantification of lithic use-wear using laser profilometry: a method based on metrology and fractal analysis. *J. Archaeol. Sci., Lithic Microwear Method: Standard. Calibr. Innov.* 48, 15–25. <https://doi.org/10.1016/j.jas.2013.04.027>.
- Stemp, W.J., Childs, B.E., Vionnet, S., Brown, C.A., 2009. Quantification and discrimination of lithic use-wear: surface profile measurements and length-scale fractal analysis*. *Archaeometry* 51, 366–382. <https://doi.org/10.1111/j.1475-4754.2008.00404.x>.
- Stemp, W.J., Stemp, M., 2001. UBM laser profilometry and lithic use-wear analysis: a variable length scale investigation of surface topography. *J. Archaeol. Sci.* 28, 81–88. <https://doi.org/10.1006/jasc.2000.0547>.
- Stout, K.J., Dong, W.P., 1994. Three Dimensional Surface Topography: Measurement, Interpretation, and Applications: A Survey And Bibliography. Penton Press, London.
- Thér, R., 2020. Ceramic technology: how to reconstruct and describe pottery-forming practices. *Archaeol. Anthropol. Sci.* 12, 172. <https://doi.org/10.1007/s12520-020-0131-0>.
- Thér, R., Wilczek, J., 2022. Identifying the contribution of rotational movement in pottery forming based on statistical surface analysis. *Archaeol. Anthropol. Sci.* 14, 98. <https://doi.org/10.1007/s12520-022-01561-y>.
- Van Dooselaere, B., 2010. Poterie et histoire au temps des grands empires uest africains: études technologiques de l’assemblage céramique de Koumbi Saleh (Mauritanie 6e–17e siècles) (Ph.D. thesis). Université Paris 1—Panthéon Sorbonne, Paris.
- Whitehouse, D.J., 1994. Handbook of surface metrology. Institute of Physics Pub, Bristol.
- Whitehouse, D.J., 2002. Surfaces and their measurement. Hermes Penton Ltd, London.
- Zupancich, A., Cristiani, E., Carra, M., Antonović, D., Borić, D., 2025. Mesolithic plant processing unveiled: Multiscale use-wear analysis of the ground stone tools from Vlasac (Serbia). *J. Archaeol. Sci. Rep.* 61, 104907. <https://doi.org/10.1016/j.jasrep.2024.104907>.